Journal of Materials Chemistry A

Accepted Manuscript

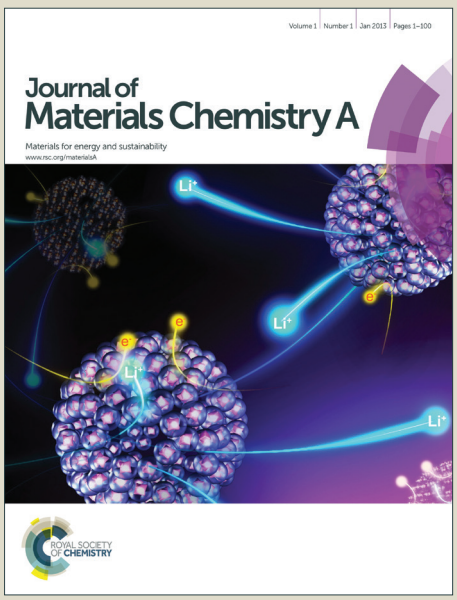

ROYAL SOCIETY OF CHEMISTRY

www.rsc.org/materialsA

Journal Name

ARTICLE

Novel fabrication of efficient solid base: carbon-doped MgO-ZnO composite and its CO_2 capture at 473 K

Received 00th January 20xx,
Accepted 00th January 20xx

DOI: 10.1039/x0xx00000x

www.rsc.org/

Yan Yan Li,[a] Mi Mi Wan,[a] Xiao Dan Sun,[a] Jun Zhou,[b] Ying Wang,[b,c] and Jian Hua Zhu*[a]

Abstract: New strategy of fabricating optimal porous strong base was reported for the first time. Magnesium and zinc acetates were mixed by microwave irradiation followed by carbonization at 823 K. Zn incorporation enabled the magnesia nanoparticles to have more surface defects, and about 80% of basic sites were the strong ones to capture CO_2 at 473 K, which is the highest proportion to date. These porous binary metal oxides had large surface areas between 130~296 $m^2 g^{-1}$.

Introduction

It is challenge to fabricate the optimal composite for social requirement, not only the low cost and environment-benign process, but also the high efficiency of the product itself. One noteworthy example is the special solid base to control CO_2 in flue gas that causes 30-40% of CO_2 emission in the world [1, 2]. The temperature of flue gas is usually over 423 K [3], it would cost lots energy-input to cool down the gas below 373 K and capture the CO_2 with conventional adsorbent ot absorbents [4]. However, directly adsorbing the CO_2 in flue gas requires special basic sorbent to capture CO_2 at 423 K or 473 K but desorb CO_2 around 673 K in order to cut down the regeneration energy, which excludes many candidates. Zeolites, hydrotalcite, amine-functionalized materials and metal organic frameworks (MOFs) fail to trap CO_2 at the elevated temperature [5-7], while Li or Ca-based capturers suffer from their high regeneration temperature (1073~1173 K) [8]. MgO is regarded as a promising candidate because of its abundant source, cheapness and appropriate basic strength [9] in comparison with ionic liquid/alumina or mesoporous Al_2O_3–ZrO_2–organosilica new adsorbents [10, 11].

It is crucial for basic sorbent to have a sufficient capability, that is, the amount of CO_2 captured by the sample of per gram at elevated temperature such as 473 K [9]. MgO itself has a small value because of its small surface area so that it has been improved through three main routes: supporting MgO on porous material, pore-creating of MgO, and admixing MgO with other components [12-23]. However, the well dispersed MgO often lacks enough strong basicity and the inactive support inevitably lowers the adsorption capacity of per gram sorbent [3, 12]. Pore-forming in MgO suffers from the complicated process using surfactants and solvents [3, 13], accompanied with high cost. Consequently, more attentions are paid on the admixing MgO with carbon, metal oxide or inorganic salts [5, 15-17, 24]. This method is frequently used to prepare catalyst and photo-catalyst where MgO is used as the modifier to form MgO-TiO_2 and $(ZnO)_x(MgO)_{1-x}$ [15, 18, 19], or modified with alkali metal oxide [20-23], but few investigation had been performed on MgO-based CO_2 sorbent, let alone the CO_2 capturer at 473 K. For fabrication of the special basic CO_2 sorbents, low cost and high efficiency are crucial. The former requests cheap raw materials rather than expensive ones like magnesium alkoxide [25], and the latter requires the sorbent to have a high proportion of strong basic sites that can adsorb CO_2 at 473 K. Common MgO has various surface sites to adsorb CO_2 at ambient temperature even the OH group [26] so its proportion of strong basic sites is low. Gregg and Ramsay subtly prepared the special sample of MgO from magnesium methoxide with a large surface area of 112 $m^2 g^{-1}$ [25], and it adsorbed the CO_2 of 0.64 mmol g^{-1} at 273 K but 0.24 mmol g^{-1} at 473 K so this ratio was 37%. How to increase this ratio of MgO-based sorbent? This is a real challenge not only facing the design of CO_2 sorbent in flue gas, but also involving the efficiency of solid base related to the nature of active sites and surface state, which spurs us to seek a new strategy. It is reported that low-coordination sites on the surface of MgO related to the efficient adsorptive sites [27], thus we try to create plenty of defects in magnesia through the special substitution between MgO and ZnO.

ZnO is one kind of amphoteric oxide featured on high abundance, low toxicity and photocatalytic ability [28], and it has many potential applications in electronic, catalysis and sensors [19]. Nonetheless, ZnO lacks the basic sites with basic strength $H_0 \geqq 6.8$ [29] so it could not catalyze oxidative dehydrogenation until addition of K_2O [30]. Substitution of Mg^{2+} with smaller ion radius for larger Zn^{2+} has been reported [31], which may be beneficial to induce the migration of Mg^{2+} cation and tune the surface state of magnesia to form more defects. Herein, magnesium acetate was employed to make binary metal oxide with zinc acetate, and they would be carbonized in

[a] Key Laboratory of Mesoscopic Chemistry of MOE, College of Chemistry and Chemical Engineering Nanjing University, Nanjing 210093, China E-mail: jhzhu@ nju.edu.cn
[b] College of Chemistry & Chemical Engineering, Nanjing University, Nanjing 210093, China.
[c] Ecomaterials and Renewable Energy Research Center (ERERC), Nanjing University, Nanjing 210093, China.

† Electronic Supplementary Information (ESI) available: additional structural and compositional characterizations (Fig. S1–7 and Table S1), additional CO_2 adsorption performance (Fig. S8–9). See DOI: 10.1039/x0xx00000x

nitrogen rather than air in order to suppress the CO_2 emission during the decomposition of acetate. The former salt provides newly-formed MgO accompanied with the carbon nano-particles and these MgO particles can be *in situ* separated by these carbons [9], while the latter acts as the accessory ingredient of adjusting the surface state of MgO, enhancing the defect number of MgO and elevating the proportion of its strong basic sites. These two inorganic salts were mixed with different methods including microwave irradiation, solution and grinding, followed by carbonization at 823 K. The influences of Mg/Zn ratio and preparative procedures on the structure and property of resulting composite were carefully investigated in order to select the optimal preparation method. To assess the potential application of these new basic sorbents in controlling CO_2 emission in flue gas, they were evaluated in the extremely harsh instantaneous CO_2 adsorption at 473 K as previously reported [9, 12, 13], in which the CO_2 concentration was lowered to 5% and the contact time between CO_2 and adsorbent was shorter than 2 s [9].

Experimental Section

Materials

Magnesium acetate tetrahydrate and zinc acetate dihydrate were the product of Sinopharm and J&K Chemical (China), MgO and ZnO were purchased from Shanghai Zhenxin and Shanghai Chemical Reagent, respectively. Coconut carbon with average pore size of 3–5 nm was provided by British American Tobacco [12]. All chemicals were of analytical grade and used as received without further purification.

Synthesis of carbon-doped binary metal oxide

(a) *Microwave irradiation method* 0.963 g $Mg(CH_3COO)_2{\cdot}4H_2O$ and 0.110 g $Zn(CH_3COO)_2{\cdot}2H_2O$ were first ground for 5 min and then wetted with 0.75 ml water. After the mixture was irradiated in a National NN-S570MFS microwave oven with a power of 525 W for 4 min, it was carbonized at 823 K for 2 h in N_2 [12]. The obtained solid was denoted as 82MZ where 82 is the weight percent of MgO in binary metal oxide. Similarly, other nMZ samples like 78MZ or 80MZ with different n values were prepared. To explore the impacts of irradiation time and water content, various 82MZ (t, v) samples were synthesized, where t and v represent microwave irradiation time (min) and amount of water added (ml), respectively. **(b)** *Grinding method*: $Zn(CH_3COO)_2{\cdot}2H_2O$ and $Mg(CH_3COO)_2{\cdot}4H_2O$, with different molar ratio were ground at 298 K and humidity of 45-55% for 20 min, followed by carbonization as mentioned above to give the sample of *n*MZ-g, while n signifies the calculated weight ratio of MgO in binary metal oxide, g means grinding. **(c)** *Solution-evaporation method*: $Zn(CH_3COO)_2{\cdot}2H_2O$ and $Mg(CH_3COO)_2{\cdot}4H_2O$, with the molar ratio of 1:9, were dissolved into 5 g H_2O and evaporated at 353 K overnight, followed by carbonization as mentioned above to give 82MZ-s sample where 82 meant the weight percent of MgO in the solid, s indicated solution method. Other *n*MZ-s samples such as 54MZ-s and 3MZ-s were prepared in the similar procedures.

For comparison, magnesium or zinc acetates was carbonized at 823 K to form MgO-C or ZnO-C, respectively [9]. 82MZ-air was made in the same procedure as that of 82MZ, but calcined in air. To get the mixture called MZAC, 0.5 g MgO and 0.113 g ZnO as well as 0.008 g coconut carbon were ground for 10 min.

Characterizations

Wide-angle X-ray diffraction (XRD) patterns of the samples were recorded on an XRD-6000 diffractometer (power 40 kV, 30 mA) using Cu-Kα radiation in the 2-theta range from 10° to 80°, and low-angle XRD patterns were obtained on an ARL XTRA diffractometer (40 kV, 40 mA, Cu-Kα radiation) in the 2-theta range from 0.5° to 6°. Nitrogen adsorption-desorption isotherms were measured on a Micromeritics ASAP 2020 system at 77 K, and the sample was evacuated at 573 K for 4 h prior to test. Brunauer–Emmett–Teller (BET) method was utilized to calculate the specific surface area of sample using adsorption branch acquired at a relative pressure (P/P_0) range of 0.05-0.22, and the total pore volume was estimated from the amount adsorbed at a relative pressure (P/P_0) of 0.98. Scanning electron microscope (SEM) images were obtained on Hitachi S4800 microscopes at 10 kV, 10 μA, and elemental mapping and Energy Dispersive X-Ray Spectroscopy (EDX) analysis of samples was taken on the same instrument at 20 kV, 15 μA. Transmission electron microscopy (TEM) images were collected on a JEM-1011 electron microscope operating at 200 kV [10]. High-resolution transmission electron microscopy (HRTEM) images were carried out on JEM-200CX equipment at an acceleration voltage of 200 kV. For the measurement the sample was ground into powders and dispersed into ethanol solvent, and the obtained suspensions were dripped, dried on a carbon film supported on copper mesh. Photoluminescence (PL) property was detected on a Varian Cary Eclips luminescence spectrometer with a wavelength of 325 nm as the excitation using a He-Cd laser. Elemental Analysis was conducted on vario EL II instrument. UV-visible diffuse reflection spectra was measured on Shimadzu UV3600 instrument and converted from reflection to absorbance using Kubelka-Munk method.

To assess the performance of porous samples in instantaneous CO_2 adsorption at 473 K [12], the *in situ* prepared sample after carbonization in u-type quartz tube in N_2 was kept at 473 K, and 0.164 mL of CO_2 was injected each time accompanied with carrier gas (H_2, 30 ml min^{-1}). The residual CO_2 was detected by an "online" Varian 3380 gas chromatograph and quantitatively measured by the external standard method [3]. In the cyclic CO_2 adsorption-desorption detection, once the adsorption of CO_2 was finished, the sample was allowed to re-adsorb CO_2 in the same manner aforementioned as soon as the entire desorption process (sample was directly heated from 473 K to 673 K and held at 673 K for 1h) was finished. Temperature programmed desorption (TPD) test was performed as follows: 20 mg of sample was put into a u-type quartz tube to be activated in N_2 (99.995%) at 823 K for 2 h, and then cooled to 298 K for adsorbing CO_2 as stated above, and then was purged with N_2 for 10 min. Finally it was heated from 298 K to 823 K at a rate of 8.8 K min^{-1} and maintained at 823 K for 1 h, meanwhile the liberated CO_2 was detected and recorded by an "online" Varian 3380 gas chromatograph[12].

Static adsorption of CO_2 at 298 K was performed on Micromeritics ASAP 2020 static volumetric instrument, in which samples were degassed at 573 K for 12 h before CO_2 adsorption.

The CO_2 adsorption isotherm at 423 K and 473 K was recorded also on a Micromeritics ASAP 2020 instrument [9, 13]. Prior to adsorption of CO_2, sample was degassed at 673 K for 6 h, and then was cooled down to the given temperature, followed by introduction of CO_2 to contact with sample. The CO_2 adsorption amount was then recorded according to the adsorbed volume under standard temperature and pressure (STP).

To monitor the dynamic adsorption and desorption of CO_2 on 82MZ sample, a Netzsch STA449C TG/DSC analyzer was employed. In the CO_2 adsorption experiment, 20 mg of sample was first heated under a N_2 flow (25 ml min^{-1}) at 823 K for 2 h and then cooled down to 473 K, followed by CO_2 introduction into the system (25 ml min^{-1}, 1.5 h). Meanwhile, the weight increase of sample was recorded. For the desorption of CO_2, the 82MZ sample adsorbed CO_2 at 473 K was purged under N_2 at 473 K for 1 h, and then heated to 673 K at a rate of 10 K min^{-1}, followed by holding at 673 K for 1 h. The decrease in the sample weight was also recorded. The regeneration property of 82MZ composite was performed by a cyclic CO_2 adsorption–desorption experiment. Sample was also activated as stated above and adsorbing CO_2 for 1 h at 473 K with N_2 purging for 5 min, then CO_2 desorption was performed as above. Once the first cycle was completed, sample was allowed to re-adsorb CO_2 for another cycle.

Results

Characterization of carbon-doped binary metal oxide

Figure 1 displayed the wide-angle XRD patterns of nMZ composites along with MgO-C and ZnO-C. Cubic crystalline phase of MgO appeared on the patterns of nMZ composites, with the 2-theta value of 42.9° and 62.3° corresponding to the (200) and (220) planes respectively [32], together with the wurtzite ZnO structure

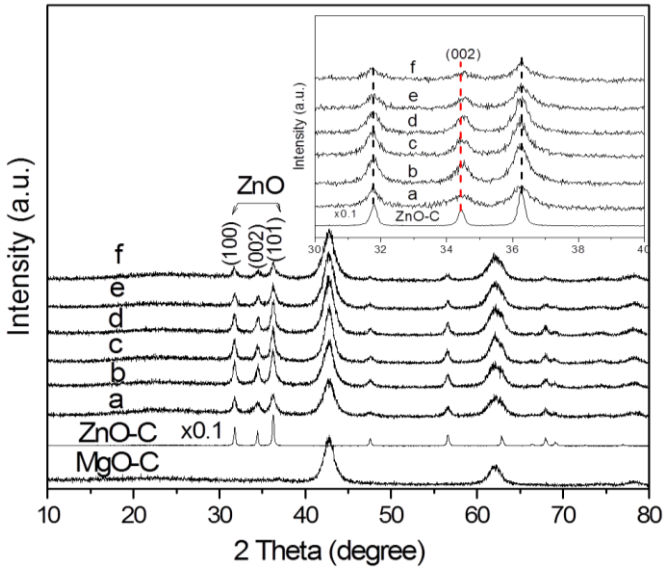

Figure 1. Wide-angle XRD patterns of (a) 78MZ, (b) 80MZ, (c) 82MZ, (d) 84MZ, (e) 86MZ, (f) 88MZ, and ZnO-C, MgO-C samples. Inset: the corresponding amplified XRD patterns.

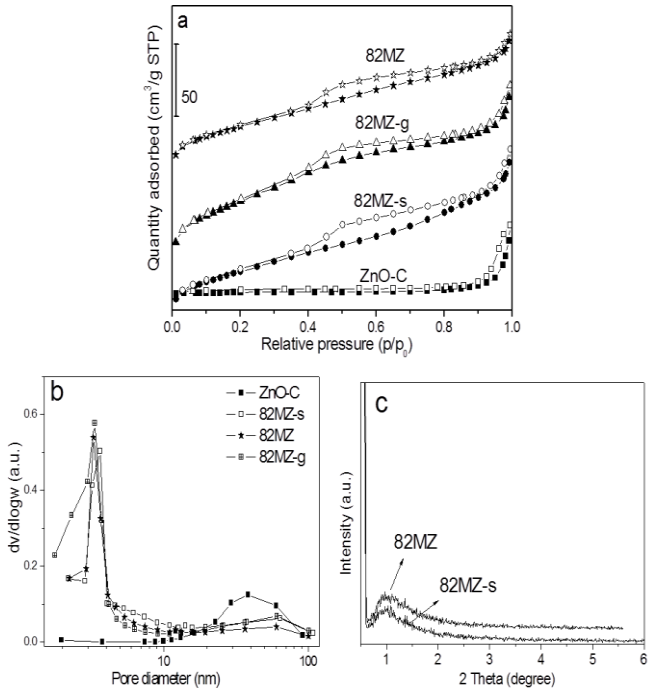

Figure 2. (a) N_2 adsorption-desorption isotherms, (b) pore-size distributions of MZ series composites and (c) low-angle XRD patterns of 82MZ and 82MZ-s samples.

value of 42.9° and 62.3° corresponding to the (200) and (220) planes respectively [32], together with the wurtzite ZnO structure with typical diffraction peaks between 2-theta value of 30° and 40° of relevant (100), (002) and (101) planes [19]. This phenomenon demonstrated certain amount of MgO and ZnO components had a phase-disengagement with each other in macrolevel [19], which was very different from that of zinc-doped MgO ($Zn_xMg_{1-x}O$) powders where no signature of ZnO phase could be identified when 10% (x = 0.1, molar ratio) of Zn was doped [33]. As shown in the inset of magnified patterns, one peak of ZnO (002) plane on nMZ samples shifted ~0.1 degree to higher angle in comparison with that of ZnO-C, and such shift of (002) peak on 88MZ was more obvious than that on 78MZ, which is very similar with $(ZnO)_x(MgO)_{1-x}$ nanoplates [19].

Similar shift was also observed on the XRD patterns of other 82MZ(t, v) composites (Fig. S1b), but absent on 82MZ-g sample. On the 82MZ-air sample which was calcined and carbon-free (Fig. S2), similar shift of ZnO (002) plane was found, indicating the major role played by microwave irradiation instead of carbon component for the shift phenomenon. These results implied the substitution of Zn^{2+} with a radius of 0.060 nm [34, 35] by the Mg^{2+} ion with a smaller radius of 0.057 nm [36]. Although 82MZ-s sample contained the same MgO content as 82MZ did, it had faintish characteristic peaks of MgO and ZnO (Fig. S1a) so that the ZnO (002) plane was indiscernible.

In the N_2 adsorption-desorption experiment, 82MZ, 82MZ-s and 82MZ-g samples presented the type IV isotherm (Fig. 2a) with H3 hysteresis loop in the relative pressure range from 0.4 to 0.9,

Table 1. Textural properties of MgO-ZnO binary oxides and their CO_2 adsorption capacities.

Samples	Pore volume ($cm^3\ g^{-1}$)	BET surface area ($m^2\ g^{-1}$)	Adsorbed CO_2 at 473 K	
			($mg\ g^{-1}$)	($mg\ m^{-2}$)
ZnO-C	0.03	8.6	0.8	0.09
MgO	0.10	35.9	1.9	0.05
78MZ-g	0.18	200.9	22.8	0.11
82MZ-g	0.18	203.1	28.2	0.14
88MZ-g	0.20	228.2	18.4	0.08
94MZ-g	0.27	295.7	19.4	0.07
82MZ-s	0.16	137.0	24.9	0.18
82MZ(4,0)	0.19	138.7	21.8	0.16
82MZ(3,0.25)	0.17	132.1	24.4	0.18
82MZ (6,0.25)	0.17	149.5	27.9	0.19
78MZ	0.13	147.7	9.7	0.07
82MZ	0.14	135.3	33.3	0.25
88MZ	0.14	166.3	14.1	0.08

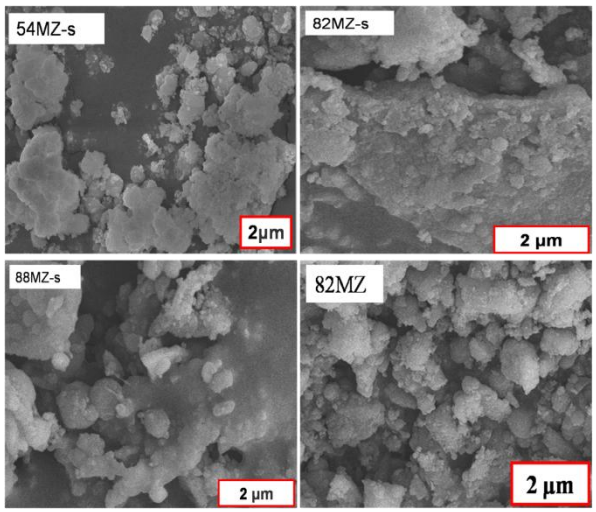

Figure 3. SEM images of 54MZ-s, 82MZ-s, 88MZ-s and 82MZ samples.

demonstrating the characteristic of disordered mesoporous structure [37, 38]. Actually they had a narrow pore-size distribution centered at 3-4 nm (Fig. 2b). Other 82MZ (t, v) and nMZ-g samples also presented the similar character of mesoporous structure as shown in Fig. S3, but ZnO-C showed a isotherm of type II with a H3 hysteresis loop in relative pressure of 0.8-1.0, signifying the presence of macroporous structure with slit-like pores [39], and it had large pores of 20-100 nm (Fig. 2b). Low-angle XRD patterns of 82MZ-s and 82MZ samples were characterized with one broad reflection peak at 2-theta value of 1° (Fig. 2c), mirroring the existence of mesoporous structure with no long-range order in pore organizations [40]. 82MZ-s and nMZ composites had the surface areas of 130~170 $m^2\ g^{-1}$, lower than that of MZ-g samples (Table 1). The surface areas and pore volumes of MZ-g raised gradually as the

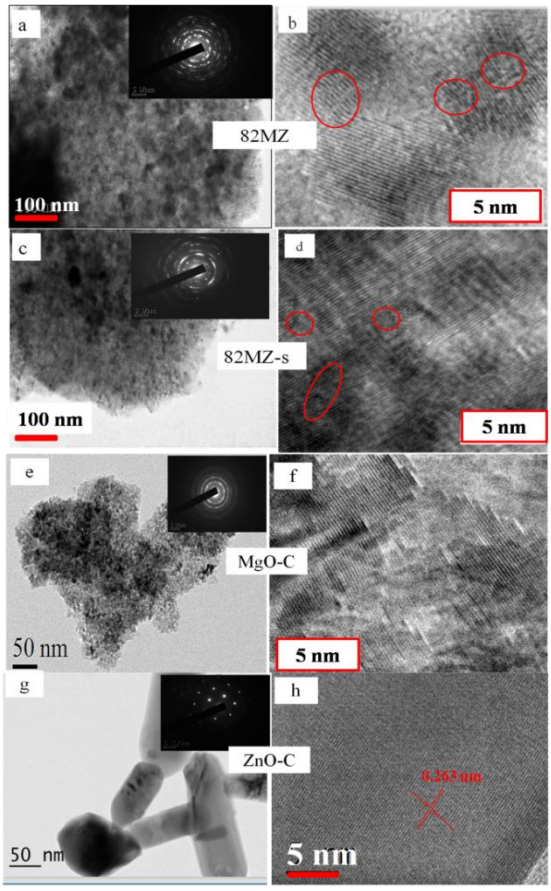

Figure 4. HRTEM images of (a) 82MZ, (c) 82MZ-s, (e) MgO-C and (g) ZnO-C samples, the insets of (a), (c), (e) (g) are the corresponding selected area electron diffractions, (b), (d), (f) and (h) are the relevant lattice fringe images.

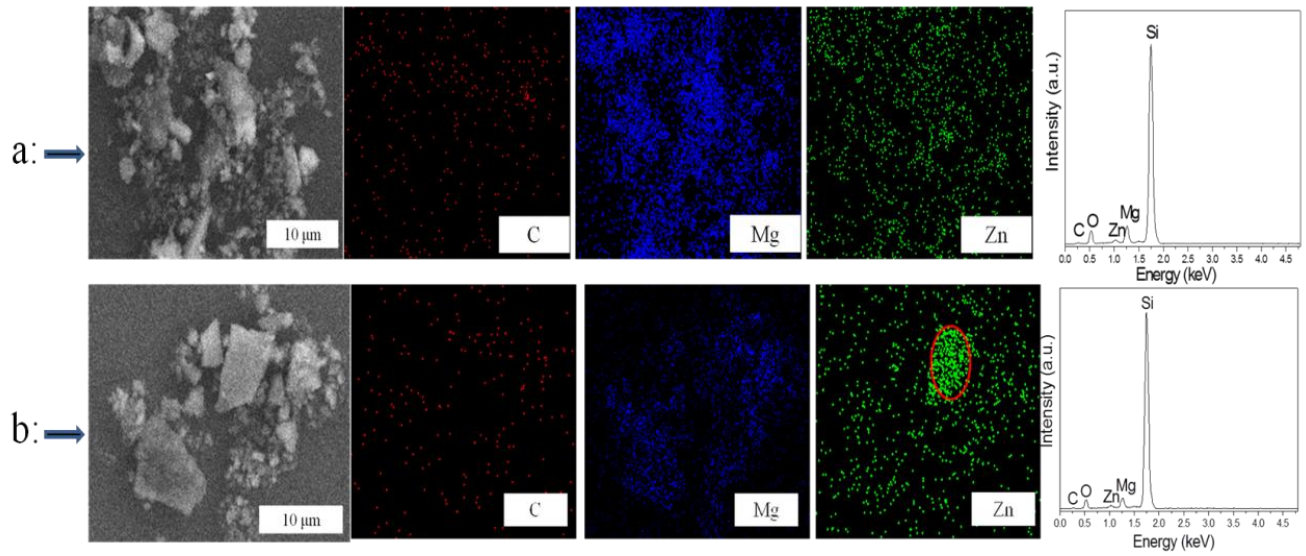

Figure 5. SEM images, X-ray mapping, and EDX spectra of (a) 82MZ and (b) 82MZ-g samples, in which the magnification is 3500 and 4000 respectively.

MgO content increased from 78% to 94%, achieved to 295.7 $m^2 g^{-1}$ and 0.27 $cm^3 g^{-1}$, close to that of carbon-inserted MgO sample [9].

82MZ and 82MZ-s samples were constituted of various small particles (Fig. 3) , but the former kept the relatively uniform sizes below 2 μm while the latter varied from 0.2 to 8 μm. Such heterogeneous particles aggregation was also found on 54MZ-s and 88MZ-s samples. According to TEM images in Fig. S5, 82MZ sample had worm-like, irregular pore structure (Fig. S5), while 82MZ-s was comprised of relatively big and round particles. Both of them contained individual particulate on their surface (Fig. 4a, 4c), but those on 82MZ-s seemed little bigger (Fig. 4c). The emergence of multiple electron diffraction rings on 82MZ and 82MZ-s (insets of Fig. 4a, 4c) demonstrated the formation of polycrystalline structure [33, 41]. In comparison with that of MgO-C sample (Fig. 4e), their new diffraction rings/spots (insets of Fig. 4a, 4c) could be indexed to ZnO diffraction patterns [33]. The diffraction rings of 82MZ-s was not as distinct and regular as that of 82MZ because of its weak crystallization (Fig. S1a). Unlike the lattice fringes of MgO-C and ZnO-C (Fig. 4f, 4h), incorporation of ZnO in 82MZ and 82MZ-s caused more disordered structures in these composites and some of the fringes twisted or disconnected (labelled with red circle) (Fig. 4b, 4d), indicating the possible alloying process of MgO with ZnO [19], which dovetailed well with the XRD results (Fig. 1). ZnO-C sample owned the single crystal structure (inset of Fig. 4g), and the lattice spacing was about 0.26 nm (Fig. 4h) that could be indexed to the (002) plane of wurtzite-structured ZnO. These results meant the growth of ZnO-C along (002) direction [42], which was the reason why merely (002) peak shift occurred in XRD pattern (Fig. 1). Element C, Mg and Zn were uniformly distributed on 82MZ and 82MZ-s samples (Fig. 5a, S6), but accumulation of Zn species was found on 82MZ-g (marked with a red ellipse, Fig. 5b) due to the non-homogeneous distribution of Zn related to grinding preparation. EDX spectra confirmed the existence of Mg, Zn and small quantity of carbon on these composites.

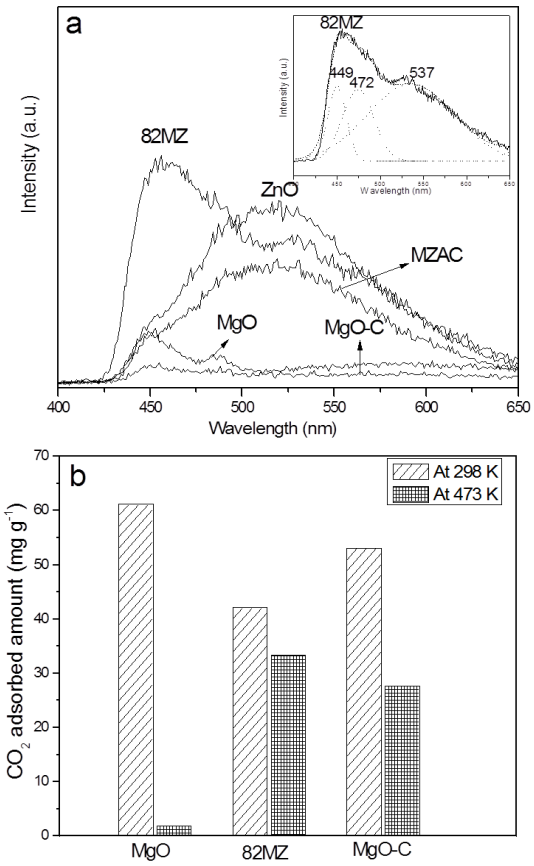

Figure 6. (a) Room-temperature PL spectrum of MgO-C, 82MZ, MgO, ZnO and MZAC samples, inset: multi peak Gaussian-fitting results of 82MZ sample. (b) CO_2 adsorption capacities on MgO-C, 82MZ and MgO samples at 298 K and 473 K.

Surface defects and vacancies directly affect the properties of MgO in adsorption, catalysis, fluorescence etc [18, 43], and in particular, they provide the necessary strong basic sites for CO_2 adsorption at 473 K [9, 27]. PL spectrum which can give the instructive evidence of

surface structural defects [13, 44] was employed to analyze the prepared samples (Fig. 6a). A remarkable enhanced PL emission was detected on 82MZ composite in comparison with that of MgO-C or ZnO (Fig. 6a), and this spectrum was deconvoluted by multi-peak Lorentzian fitting (inset of Fig. 6a) to generate three distinguished peaks at 449, 472 and 537 nm, respectively. Among them the 472 nm band was corresponding to MgO structural defects [18, 45], the broad 537 nm emission band related to oxygen vacancies of ZnO [46] on 82MZ, and the enhanced emission might mirror the recombination between interstitial Mg and zinc vacancies as Mg defects increased [47]. Apparently, the defect sites of 82MZ were much more abundant than that of MgO-C whose emission was unobvious at 485 nm (Fig. 6a), mirroring the role of ZnO as an important accessory ingredient. 82MZ sample has the same composition as MZAC mixture did, but their PL spectrum differed dramatically. The defect sites of MgO became prominent and enlarged in the former while the latter was really the mixture of PL bands of MgO, ZnO and carbon, which indicates the interactions between ternary components in 82MZ composite rather than mechanical mictures. Differently, a broad green emission band centered at 450 nm with a minor shoulder at about 485 nm was observed on MgO-C and MgO samples, which was associated with the surface OH^- in low coordination sites such as corners and edges of MgO [18], the shoulder band of 485 nm related with MgO defect sites [18]. One broad emission at roughly 518 nm on ZnO may relate to oxygen vacancies [46]. On the UV-vis adsorbence results shown in Fig. S7, ZnO-C and MZAC samples had a strong absorption in UV region around 365 nm but no obvious absorption in visible-light region while MgO-C exhibited a rather faint absorption. However, the absorption edge of 82MZ shifted to visible light region with an obviously strengthened intensity, which related to the interaction between the subject (MgO) and guest (ZnO) [48, 49].

Adsorption of CO_2 at 473 K by MgO-based composites

Instantaneous CO_2 adsorption was used to assess the basicity of MgO-ZnO composites. 82% of MgO was proven to be optimal for MZ sample no matter it was prepared through microwave irradiation, grinding or solution procedure (Table 1, Fig. S8), and 82MZ could capture 33 mg g^{-1} of CO_2 at 473 K. This value exceeded that of MgO (1.9 mg g^{-1}) or carbon-inserted MgO (28 mg g^{-1}) [9]. 82MZ sample contained about 1.2% of carbon (Table S1) and about 82% of MgO, that is, 1 g MgO in this composite can capture 33.3/0.82 = 40.6 mg g^{-1} of CO_2 at 473 K, which is the highest efficiency of MgO to date [9, 12, 25]. Lowering the water content or irradiation time in the preparation of 82MZ (t,v) sample only caused a minor effect since these composites kept the adsorption capacities of 24~31 mg g^{-1} (Fig. 7a). Without water added, 82MZ (4, 0) sample still adsorbed 21.8 mg g^{-1} of CO_2 at 473 K (Table 1). For the samples prepared through solution-evaporation, their CO_2 adsorption capacities increased as the content of MgO raised from 5% to 82% (Fig. S8a), reached a climax of 24.9 mg g^{-1} on 82MZ-s (Table 1). Further increasing MgO content could not elevate the adsorption. Similar circumstance happened on MZ-g samples (Fig. S8b), among them 82MZ-g was also the champion to adsorb CO_2 of 28.2 mg g^{-1} at 473

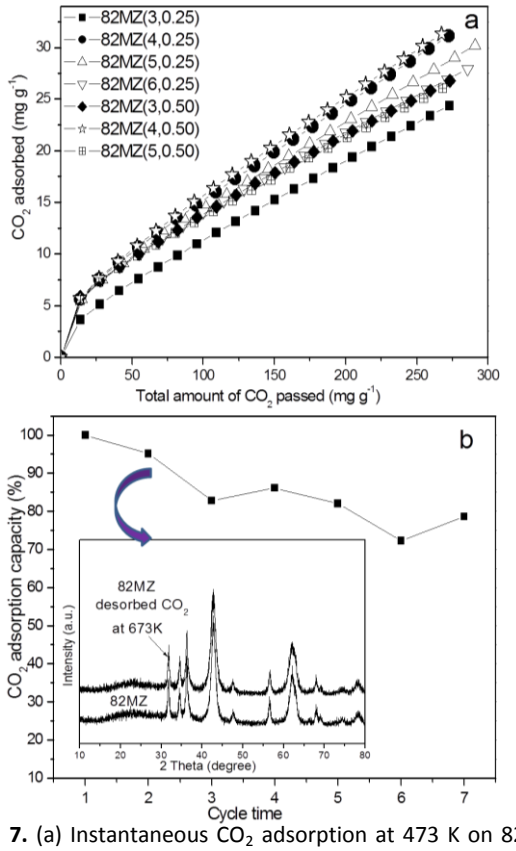

Figure 7. (a) Instantaneous CO_2 adsorption at 473 K on 82MZ(t, v) samples, (b) Cyclic CO_2 adsorption on 82MZ sample at 473 K. Inset of b is the wide-angle XRD pattern of 82MZ after CO_2 desorption at 673 K.

K. ZnO-C could hardly adsorb CO_2 (Table 1, Fig. S8a), because of its small surface area and amphoteric character.

Since only the top layer of MgO can contact with CO_2, it is important to calculate the efficiency of sorbent by the amount of CO_2 trapped on per unit of surface area [3]. According to the data in Table 1, 82MZ owned the highest value of 0.25 mg m^{-2}, 4 times larger than that of MgO (0.05 mg m^{-2}). Next, three 82MZ(t, v) series samples, including 82MZ(6, 0.25), (3, 0.25) and (4, 0) along with 82MZ-s, showed a large value of 0.16~0.19 mg m^{-2}, double higher than that of MgO (Table 1). Besides, 82MZ composite showed a good performance in the 7th adsorption-desorption cycles (Fig. 7b), keeping about 70% of the original adsorption capacity within the experimental error. Its structure kept stable without phase variation after CO_2 adsorption at 473 K and desorption at 673 K (inset of Fig. 7b).

TGA analysis was performed on 82MZ sample to get real kinetics of CO_2 capture. Its adsorption can divide into two stages (Fig. 8a): the first is a quick adsorption and 33% of the total adsorption is achieved within 9 min. After 19 min of exposure to CO_2, the sample weight increased 1%, achieving to half of the total adsorption. The residual half needed another 70 min with a relatively low adsorption rate (Fig. 8a). During TGA analysis, the sample was put into the crucible with an inner diameter of 0.65 cm and length of 1.3 cm (inset of Fig. 8a), CO_2 was purged from the bottom up and contacted with the sorbent into the crucible through diffusion,

which caused a lower adsorption rate within the first 19 min at 473 K than the adsorbents of KCC-1-N700 etc at 298 K [50]. Besides, the adsorption rate appeared first quick back slow trend overall, since CO_2 was firstly adsorbed on the surface affinity sites of 82MZ, the rest adsorption sites in the bottom were not easily accessible, therefore the adsorption rate decreased a lot in the subsequent 70 min. Besides the different adsorption temperature (473 K and 298 K, this is the deadly difference), is the intrinsic reason for the lower adsorption rate of diffusion-controlled MgO-based adsorbent than KCC-1-N700 [50].

The CO_2 desorption finished within 23 min (Fig. 8a), and almost all of the adsorbed species were desorbed from 82MZ composite at 673 K. Compared with some CaO-based adsorbents [8], the low regeneration temperature of 82MZ is very advantageous for saving energy and time. Yet, the adsorption capacity of 82MZ sample at

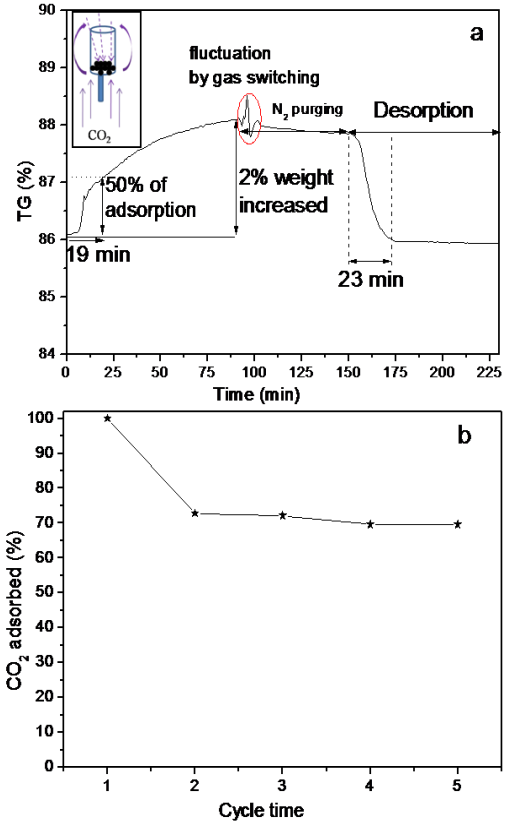

Figure 8. (a) TGA analysis on 82MZ sample for CO_2 adsorption at 473 K and desorption from 473 K to 673 K (kept at 673 K for 1 h). Inset is the contact mode between 82MZ and CO_2 in curcible during TGA analysis, (b) cyclic CO_2 adsorption-desorption on 82MZ in TGA analysis.

473 K during this TGA analysis was 20 mg g^{-1}, 61% of that in instantaneous CO_2 adsorption. One reason for the different results is the flow manner of carry gas. The gas flow passes throughout the u-type quartz tube containing sample in the instantaneous CO_2 adsorption and thus all particles of the sample can contact with CO_2 in the gas stream while in the TGA test, the gas flow passes through the crucible so that only the particles located on the surface of sample can contact with the adsorbate. Obviously, the sample lacks the adequate contact with CO_2 in the TGA experiment as that in the instantaneous CO_2 adsorption.

Continual adsorption–desorption cycles of 82MZ sample in TGA was also studied (Fig. 8b). After one cycle, the adsorption amount of the sorbent decreased to 73% of the initial value, but kept the stable value basically in the following adsorption-desorption process. After 5th cycle, 82MZ composite could keep 70% of the original ability (Fig. 8b). Actually, the reuse capability of 82MZ at 473 K was inferior to that of KCC-1-N700 etc at 298 K [50] because the high adsorption temperature such as 473 K is deadly for CO_2

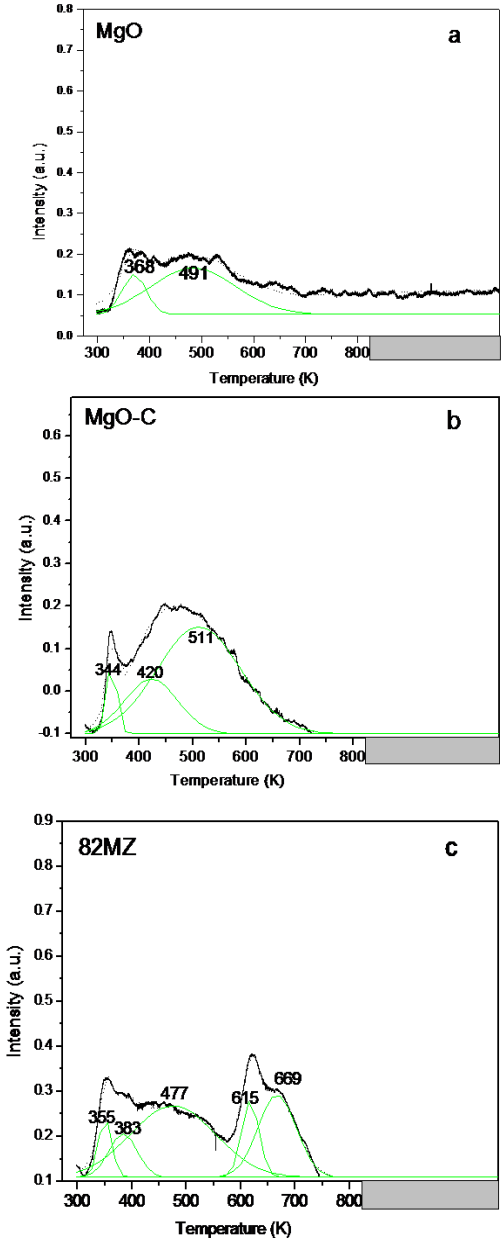

Figure 9. CO_2-TPD profiles of (a) MgO, (b) MgO-C and (c) 82MZ samples measured from 298 to 823 K at a rate of 8.8 K min^{-1} and was held at 823 K for 1 h.

adsorbent. Also, $MgCO_3$ layer may be formed once CO_2 reacted with MgO at 473 K. These layers covered on the surface of MgO and

prevented the further reaction of MgO towards CO_2, which is a common drawback for MgO-based adsorbents.

CO_2-TPD experiment can give instructive evidence on the amount and strength of basic sites of sorbent, thus it was utilized on MgO, MgO-C and 82MZ composites as displayed in Fig. 9.

Three corresponding TPD curves were deconvoluted by multi-peak Gauss fitting method, generating several distinguished peaks at different temperatures. Two desorption peaks appeared at 368and 491 K on MgO (Fig. 9a), representing the weak and middle strong basic sites, respectively [13]. Also, MgO-C sample has the similar basic species, but its basic strength is much stronger in comparison with MgO (Fig. 9b). Once ZnO was incorporated into 82MZ, the climax of desorption peaks shifted towards the high temperature of 615 and 669 K (Fig. 9c), and these basic sites can be ascribed to medium-strong ones [13], which was very significant for 82MZ to capture CO_2 at 473 K while desorbing CO_2 at 673 K. Moreover, the kinds of basic sites on 82MZ increased a lot than MgO and MgO-C samples, which dovetailed nicely with PL results (Fig. 6a). The percentage of basic sites on 82MZ sample could be calculated through peak area integral. The medium-strong basic sites with desorption peaks centered at 477 K - 669 K account for 84% of the total basic sites on 82MZ composite, which is very helpful for the sorbent to capture CO_2 at 473 K.

Static adsorption of CO_2 was conducted on 82MZ to have an overall assessment on the basic composite. The quantity of CO_2 adsorbed at 423 and 473 K positively correlated with the pressure, achieving to 36.2 and 32.5 mg g^{-1} separately at standard pressure (Fig. 10a). Due to the exothermic process of CO_2 adsorption, the adsorption capability of 82MZ at 473 K was inferior to that of 423 K, but its capacity at 473 K in this static condition (32.5 mg g^{-1}, Fig. 10a) inosculated well with the value of instantaneous adsorption (33.3 mg g^{-1}, Table 1). When the CO_2 of 4.7 cm^3 g^{-1} (STP) wasadsorbed on 82MZ, the isosteric heat of adsorption achieved the value of 27.8 KJ mol^{-1} (Fig. 10a). However, as the amount of CO_2 reached 15 cm^3 g^{-1} (STP), lower adsorption heat of 4.9 KJ mol^{-1} was obtained due to the existence of different basic sites [13]. CO_2 adsorption was also performed on MgO, MgO-C and 82MZ samples at 298 K, in which their adsorption capacities increased as the CO_2 pressure rose (Fig. 10b). It is worth noted that MgO is the champion in the CO_2 adsorption at 298 K, but the whipper-in at 473 K (1.9 mg g^{-1}, Table 1).

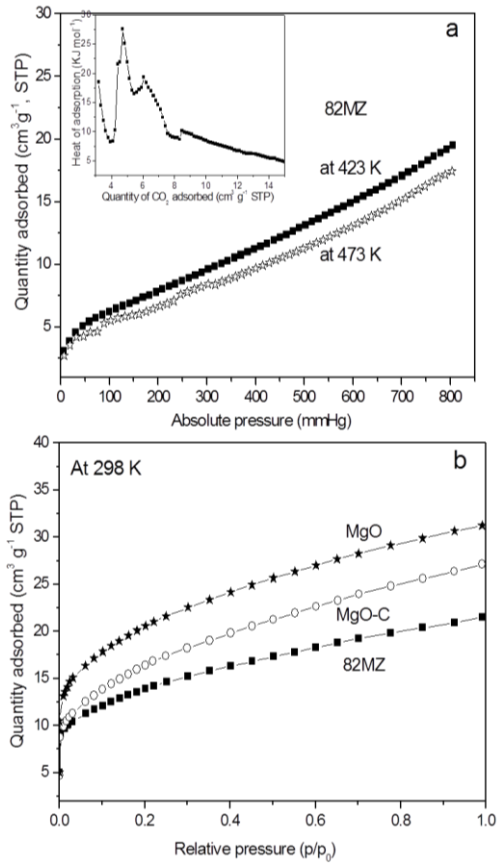

Figure 10. (a) The isotherms of CO_2 adsorption at 423 and 473 K on 82MZ sample, inset is the isosteric heat of adsorption on this sample, (b) isotherms of CO_2 adsorption at 298 K on MgO, MgO-C and 82MZ samples.

Discussion

It is meaningful to compare the discrepancy between CO_2 adsorption capacities of MgO, MgO-C and 82MZ at 298 K and 473 K, in order to obtain the instructive evidences on the roles played by the new-formed carbon and more importantly, the ZnO modifier. The adsorption capacity at 298 K originates from the contribution of all basic sites while that at 473 K only comes from strong basic sites therefore the proportion of strong basic sites in sorbent can be estimated through this difference. MgO, MgO-C and 82MZ samples adsorbed 61.2, 53.1 and 42.1 mg g^{-1} CO_2 at 298 K (Fig. 6b) but 1.9, 27.7 and 33.3 mg g^{-1} at 473 K hence their ratios of strong basic sites are 3%, 52% and 79%, respectively. MgO-C sample contains some carbon nano-particles that *in situ* separate the MgO particles so that it has a higher ratio of strong basic sites (52%) than that of the MgO made from expensive magnesium methoxide (0.37, [25]). The 82MZ sample consists of less carbon nano-particles (1.2%) and MgO (about 82%) than MgO-C (2.5%, 87.5%) but it exhibited a higher ratio of strong basic sites owing to the crucial interaction with ZnO modifier.

Substitution of Zn^{2+} by Mg^{2+} in 82MZ sample changed its surface state. The position of (002) crystalline plane of ZnO slightly shifted to a higher 2-theta angle on 82MZ sample (Fig. 1), due to the substitution of Mg^{2+} with smaller ion radius for larger Zn^{2+} [31]. ZnO composite can be prepared with preferred c-axis (002) orientation in special synthesis or particular substrate [51, 52], resulting in the enhanced properties since preferred (002) orientation along the c-axis of ZnO is a denotation of the minimization of internal strain, surface free energy and closed-packed arrangements of atoms [51]. Herein, MgO acted as a "substrate", and ZnO interacted with the "substrate" through (002) plane along c-axis (Scheme 1), in which the small Mg^{2+} substituted Zn^{2+} and leading to the shift of (002) peaks in Fig. 1. Besides, the displacement of Zn^{2+} by Mg^{2+} caused the vacancies or defects in MgO lattice (Scheme 1), increasing the number of low-coordinated O^{2-} defect sites (Fig. 6a) and enhancing

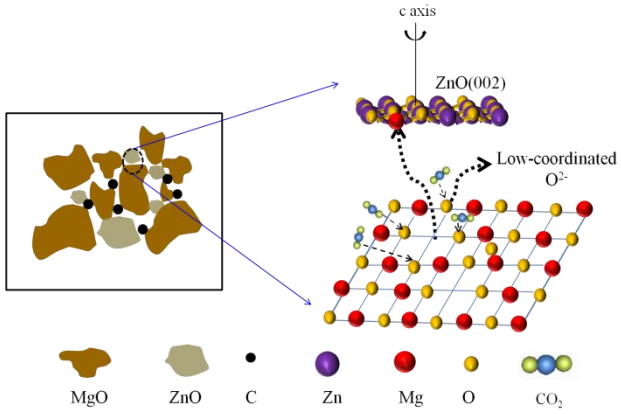

Scheme 1. Possible mechanism of the enhanced CO_2 adsorption on 82MZ sample through carbon-insertion and substitution of Zn^{2+} with Mg^{2+}.

the proportion of strong basic sites to 79% in 82MZ composite, far beyond that of MgO. Chemisorption plays a dominant role in capturing CO_2 at 473 K, even though MgO surface had different defect sites [27], CO_2 was chemisorbed and formed carbonate species on these low-coordinated O^{2-} defect sites [53], therefore the increased low-coordinated O^{2-} defect sites was beneficial for 82MZ in CO_2 capture at 473 K.

It was very important for MgO to keep original crystals and exposure of defects for adsorbing CO_2 at elevated temperature [9], which is really realized on 82MZ: firstly, the *in situ* formed carbon nano-particles separated MgO and ZnO in integrated crystals as testified in Fig. 1 where all of the characteristic of MgO and ZnO were well presented, unlike the single-phase with only preferred orientation along c-axis of the $Co_{0.2}Mg_xZn_{0.8-x}O$ films [31]. Secondly, but mostly important, added ZnO component increased the defects of MgO adsorbent (Scheme 1), thus elevated the proportion of strong basic sites for adsorbing CO_2 at 473 K. It is the specific separation and modulation of incorporated ZnO and *in situ* formed carbon that endow 82MZ an effective CO_2 adsorption capability.

Two factors impact the carbon-doped MgO-ZnO composite to be optimized basic sorbent: one is the optimized incorporation of Zn, and another is the preparation process. Zn incorporation in MgO is definitely important since it can increase the abundance of defect sites (Fig. 6a), but its amount should be optimized: ZnO-C had a small surface area and pore volume (Table 1) so that its introduction was unfavorable for enlarging the surface area of sorbent. 18% of ZnO incorporation enabled nMZ-s, nMZ-g and nMZ to efficiently adsorb CO_2 at 473 K (Fig. S8, Table 1), but this amount of ZnO (that is 10 mol%) was lower than the solubility limit of ZnO in binary MgO-ZnO composites at high temperature (28 mol%, [33, 54]). By this token, ZnO crystalline peak should be absent in the wide-angle XRD patterns of 82MZ. However, all 82MZ-x composites presented the characteristic peaks of ZnO (Fig.1 and Fig. S1a), probably due to the "carbon insertion" in the composite [9]. These new-formed carbon extra-fine particles, with a weight ratio of 1-2% (Table S1), admixed with MgO and ZnO to separate them [9]. Consequently, the ZnO component had phase-separated (Fig. 1 and Fig. S1a) with MgO even its molar percentage below the solubility limit (about 28 mol% [54]).

Preparation of MgO-ZnO composites is very important to determine their structure and property. Microwave irradiation enabled magnesium and zinc acetates to be properly mixed and interacted with the assistance of suitable water [55], and they could form eutectic salts with similar decomposition temperature, therefore the newly-formed carbon could well isolate the simultaneously produced MgO and ZnO particles, producing 82MZ with an unexpected proportion of strong basic sites (Fig. 6b). The drawback of grinding method is its poor repeatability (Fig. S9) and the unequal distribution of Zn species (Fig. 5b), no substitution of Zn^{2+} by Mg^{2+} was signified in crystal lattice (Fig. S1b). ZnO acted as merely an adulterant so that the MZ-g samples showed a low CO_2 adsorption efficiency of 0.07~0.14 mg m^{-2} (Table 1). During evaporation of solution, acetate anions can hydrolyze into CH_3COOH and OH^- within chemical equilibrium, and some Mg and Zn cations turn into $Mg(OH)_2$ and $Zn(OH)_2$ [19]. $Zn(OH)_2$ decomposes to form ZnO around 413 K [56] but the thermal-decomposition of $Mg(OH)_2$ takes place at about 573 K [57]. Thus, the production of MgO and ZnO in the sample was asynchronous so that the newly-formed carbon could not separate MgO and ZnO simultaneously, and the pre-produced ZnO might aggregate together as temperature increased up to 823 K (Fig. 3). Thus, 82MZ-s sample had a weak crystalline structure (Fig. S1a, inset of Fig. 4c) along with the lower CO_2 adsorption ability (24.9 mg g^{-1}, Table 1) than 82MZ and 82MZ-g.

Apart from the efficient CO_2 adsorption of 82MZ sample at 473 K, suppress of CO_2 emission in its preparation cannot be ignored. 340 mg precursor of 82MZ (equaling to 94 mg of the sorbent) released 232 mg CO_2 in the calcination in air but 104 mg in the carbonization in nitrogen, that means, carbonization of the acetates suppressed 44% of CO_2 emission so that production of every gram of the sorbent is accompanied with the CO_2 emission reduction of (232-104)/94=1.4 g. Moreover, 82MZ sample contains the carbon of 12 mg g^{-1} that can form CO_2 of 44 mg. These efforts are beneficial for suppressing the CO_2 emission at source.

Conclusion

New porous strong bases, carbon-doped MgO-ZnO, have been successfully fabricated from magnesium acetate and zinc acetate. Two cheap acetates were well mixed through microwave irradiation, followed by carbonization at 823 K to form the optimal mesoporous basic composites like 82MZ with a large surface area of 130~296 m^2 g^{-1}.

Owing to the addition of ZnO and its interaction with MgO, new composite such as 82MZ has abundant basic sites. Among them, 79% are strong basic sites that can capture CO_2 at 473 K and this proportion achieves the highest value to date.

Acknowledgements

Financial supports from NSF of China (21173117 and 21273106), and Analysis Center of Nanjing University are gratefully acknowledged.

Notes and references

1 J. Tollefson and R. Monastersky, *Nature*, 2012, **491**, 654.
2 M. Mikkelsen, M. Jorgensen and F. C. Krebs, *Energy Environ. Sci.*, 2010, **3**, 43.
3 K. K. Han, Y. Zhou, Y. Chun and J. H. Zhu, *J. Hazard. Mater.*, 2012, **203– 204**, 341.
4 H. W. Pennline, D. R. Luebke, K. L. Jones, C. R. Myers, B. I. Morsi, Y. J. Heintz and J. B. Ilconich, *Fuel Process Technol.*, 2008, **89**, 897.
5 D. P. Bezerra, F. W. M. d. Silva, P. A. S. d. Moura, A. G. S. Sousa, R. S. Vieira, E. Rodriguez-Castellon and D. C. S. Azevedo, *Appl. Surf. Sci.*, 2014, **314**, 314.
6 J. An and N. L. Rosi, *J. Am. Chem. Soc.*, 2010, **132**, 5578.
7 N. N. Linneen, R. Pfeffer and Y. S. Lin, *Chem. Eng. J.*, 2014, **254,** 190.
8 J. M. Valverde, P. E. Sanchez-Jimenez, L. A. Perez-Maqueda, M. A. S. Quintanilla and J. Perez-Vaquero, *Appl. Energy*, 2014, **125**, 264.
9 Y. Y. Li, M. M. Wan, W. G. Lin, Y. Wang and J. H. Zhu, *J. Mater. Chem. A*, 2014, **2**, 12014.
10 M. M. Wan, H. Y. Zhu, Y. Y. Li, J. Ma, S. Liu and J. H. Zhu, *ACS Appl. Mater. Interfaces*, 2014, **6**, 12947.
11 C. Gunathilake and M. Jaroniec, *J. Mater. Chem. A*, 2015, **3**, 2707.
12 Y. Y. Li, K. K. Han, W. G. Lin, M. M. Wan, Y. Wang and J. H. Zhu, *J. Mater. Chem. A*, 2013, **1**, 12919.
13 K. K. Han, Y. Zhou, W. G. Lin and J. H. Zhu, *Micropor. Mesopor. Mater.*, 2013, **169**, 112.
14 G. Xiao, R. Singh, A. Chaffee and P. Webley, *Inter. J. Greenhouse Gas Control*, 2011, **5**, 634.
15 Q. Li, L. Zong, C. Li and J. Yang, *Appl. Surf. Sci.*, 2014, **314**, 458.
16 A. M. Foller, Magnesium Oxide and its Applications, Vollhardt, Berlin, 1978.
17 V. R. Choudhary, V. H. Rane and S. T. Chaudhari, *Catal. Lett.*, 1990, **6**, 95.
18 M. Anpo, S.-C. Moon, K. Chiba, G. Martra's and S. Coluccia, *Res. Chem. Itermed.*, 1993, **19**, 495.
19 J. Lian, C. Zhang, Q. Li and D. H. L. Ng, *Nanoscale*, 2013, **5**, 11672.
20 W. C. Choi, J. S. Kim, T. H. Lee and S. I. Woo, *Catal. Today*, 2000, **63**, 229.
21 D.-E. Jiang, B. Zhao, Y. Xie, G. Pan, G. Ran and E. Min, *Appl. Catal. A: General*, 2001, **219**, 69.
22 P. Thomasson, O.S. Tyagi and H. Knozinger, *Appl. Catal. A: General*, 1999, **181**, 181.
23 S. Kus, M. Otremba, A. Torz and M. Taniewski, *Fuel*, 2002, **81**, 1755.
24 S. J. Han, Y. Bang, H. J. Kwon, H. C. Lee, V. Hiremath, I. K. Song and J. G. Seo, *Chem. Eng. J.*, 2014, **242**, 357.
25 J. V. Evans and T. L. Whateley, *Trans. Faraday Soc.*, 1967, **63**, 2769.
26 S. J. Gregg and J. D. Ramsay, *J. Chem. Soc. A*, 1970, 2784.
27 S. Coluccia, A. Bartona and A. Tench, *J. Chem. Soc., Faraday Trans. 1*, 1981, **77**, 2203.
28 F. Wang, L. Liang, L. Shi, M. Liu and J. Sun, *Dalton Trans.*, 2014, **43**, 16441.
29 T. Yamanaka and K. Tanabe, *J. Phys. Chem.*, 1976, **80**, 1723.
30 M. Ai, *J. Catal.*, 1977, **50**, 291.
31 Y.-J. Lin, C.-L. Tsai, C.-J. Liu, L. Horng, Y.-T. Shih, M.-S. Wang, C.-S. Jhang and C.-S. Huang, *J Sol-Gel Sci. Technol.*, 2009, **52**, 109.
32 H. S. Jung, J.- K. Lee, M. Nastasi, S.- W. Lee, J.- Y. Kim, J.- S. Park, K. S. Hong and H. Shin, *Langmuir*, 2005, **21**, 10332.
33 H. Zhang, A. R. Gheisi, A. Sternig, K. Muller, M. Schowalter, A. Rosenauer, O. Diwald and L. Madler, *ACS Appl. Mater. Interfaces*, 2012, **4**, 2490.
34 P. Shimpi, P.-X. Gao, D. G. Goberman and Y. Ding, *Nanotechnology*, 2009, **20**, 125608.
35 G. N. Panin, A. N. Baranov, Y.-J. Oh and T. W. Kang, *Current Appl. Phys.*, 2004, **4**, 647.
36 R. D. Shannon, *Acta Cryst.*, 1976, **A32**, 751.
37 C. Yu, L. Zhang, J. Shi, J. Zhao, J. Gao and D. Yan, *Adv. Funct. Mater.*, 2008, **18**, 1544.
38 S.-W. Bian, J. Baltrusaitis, P. Galhotra and V. H. Grassian, *J. Mater. Chem.*, 2010, **20**, 8705.
39 W.-C. Li, A.-H. Lu, C. Weidenthaler and F. Schuth, *Chem. Mater.*, 2004, **16,** 5676.
40 Z. Zhang and T. J. Pinnavaia, *J. Am. Chem. Soc.*, 2002, **124**, 12294.
41 Z, Zhao, H. Dai, Y. Du, J. Deng, L. Zhang and F. Shi, *Mater. Chem. Phys.*, 2011, **128**, 348.
42 H. Lu, F. Zheng, M. Guo and M. Zhang, *J. Alloy. Compd.*, 2014, **588**, 217.
43 M. Chiesa, M. C. Paganini, E. Giamello, D. M. Murphy, C. D. Valentin and G. Pacchioni, *Acc. Chem. Res.*, 2006, **39**, 861.
44 H.-B. Lu, L. Liao, H. Li, Y. Tian, D.-F. Wang, J.-C. Li, B.-P. Zhu and Y. Wu, *Solid State Commun.*, 2008, **147**, 57.
45 Y. F. Hao, G. W. Meng, C. H. Ye, X. R. Zhang and L. D. Zhang, *J. Phys. Chem. B*, 2005, **109**, 11204.
46 H. W. Kim, S. H. Shim and C. Lee, *Mat. Sci. Eng. B*, 2007, **136**, 148.
47 S. Chawla, K. Jayanthi, H. Chander, D. Haranath, S. K. Halder and M. Kar, *J. Alloy. Compd.*, 2008, **459**, 457.
48 Y.-P. Zhu, M. Li, Y.-L. Liu, T.-Z. Ren and Z.-Y. Yuan, *J. Phys. Chem. C*, 2014, **118**, 10963.
49 C. Han, L. Ge, C. Chen, Y. Li, X. Xiao, Y. Zhang and L. Guo, *Applied Catalysis B: Environmental*, 2014, **147**, 546.
50 U. Patil, A. Fihri, A.-H. Emwas and V. Polshettiwar, *Chem. Sci.*, 2012, **3**, 2224.
51 M. F. Malek, M. H. Mamat, Z. Khusaimi, M. Z. Sahdan, M. Z. Musa, A. R. Zainun, A. B. Suriani, N. D. M. Sin, S. B. A. Hamid and M. Rusop, *J. Alloy. Compd.*, 2014, **582**, 12.
52 R. Shabannia and H. A. Hassan, *Mater. Lett.*, 2013, **98**, 135.
53 A. Chakradhar and U. Burghaus, *Surf. Sci.*, 2013, **616**, 171.
54 E. R. Segnit and A. E. Holland, *J. Am. Ceram. Soc.*, 1965, **48**, 409.
55 Y. Ju and R. S. Varma, *Green Chem.*, 2004, **6**, 219.
56 S. V. Nistor, D. Ghica, M. Stefan, I. Vlaicu, J. N. Barascu and C. Bartha, *J. Alloy. Compd.*, 2013, **548**, 222.
57 J. Green, *J. Mater. Sci.*, 1983, **18**, 637.

Graphical Abstract

Novel fabrication of efficient solid base: carbon-doped MgO-ZnO composite and its CO_2 capture at 473 K

Yan Yan Li, Mi Mi Wan, Xiao Dan Sun, Jun Zhou, Ying Wang and Jian Hua Zhu

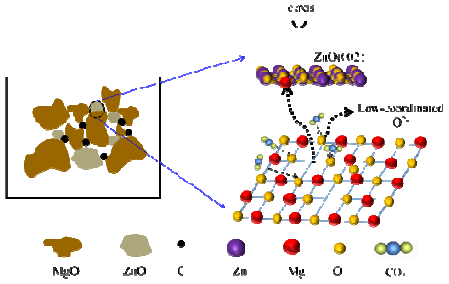

A new facile strategy of "surface vacancy" for fabricating carbon-doped MgO-ZnO composite with unwonted strong basicity is first reported, which presents well instantaneous CO_2 adsorption at 473 K.